Effect of Plunging Oscillation on an Offshore Wind Turbine Blade Section

F. Rasi Marzabadi

Abstract—A series of experiments were carried out to study unsteady behavior of the flow field as well as the boundary layer of an airfoil oscillating in plunging motion in a subsonic wind tunnel. The measurements involved surface pressure distribution complimented with surface-mounted hot-films. The effect of leading-edge roughness that simulates surface irregularities on the wind turbine blades was also studied on variations of aerodynamic loads and boundary layer behavior.

Keywords—Boundary layer transition, plunging, reduced frequency, wind turbine.

I. INTRODUCTION

THE first accepted establishment of the use of wind turbines was in the tenth century in Persia [1]. With the advent of the industrial era, wind mills were practically relegated to pump water for agricultural use. In the 20th century, new designs enabled electricity generation [2]. Denmark, Germany, the Netherland and the USA had a great influence on the development of wind turbines [3]. The increasing demand for energy, global warming, air and other pollutions, safety, cost, and the large amount of energy found in waves and wind, have motivated the search for renewable energy sources. The UK, Japan, Norway, Sweden, France and the USA were pioneers. Day by day, the demand for energy has increased. The European Union has a target to make 22.1% of its electricity by 2020 from renewable energy, as in the Kyoto protocol [4]. Vast deepwater wind resources represent the potential use of offshore wind turbines to power much of the world with renewable energy [5]. Wind turbines should be designed for different conditions, such as operational and survival conditions. Offshore wind turbine rotors as well as onshore ones are subjected to large time dependent variations in angle of attack as a result of the control input angles, periodic variations in local velocity, blade flapping, structural response and the wake inflow. Thus, the unsteady aerodynamic behavior of the blade sections must be properly understood to enable accurate predictions of the air loads of the rotor system and analyzing the dynamic response of floating structures. One unsteady, nonlinear aerodynamic problem of particular significance on wind turbines is dynamic stall. This is a transient stall effect that can result in unsteady aerodynamic forces being produced and are considerably in excess of what would be expected or predicted under steady conditions [6]. Dynamic stall phenomenon has been extensively studied experimentally, mostly using oscillating two-dimensional airfoils in wind tunnels [7-11]. The majority of the documented experimental results are for airfoils oscillating in pitch. There exist limited amounts of data available for another type of motions, such as plunging oscillation. Most of the angle of attack changes that the rotor blades encounter are due to the variations in flapping and elastic bending of the blade, which can be closely modeled with a plunging type motion.

Furthermore, dirt and contaminations accumulate on the wind turbine blade when it operates in the field. The main sources of contamination are insect compacts, ageing, sand impacts and the contaminations which come down with the rain. This contamination has a great role on the rotor performance. When insects, smog and dirt accumulate along the leading edge of the blade, power output can drop up to 40% of its clean value [12]. Surface roughness reduces the effectiveness of the airfoil. In this way the transition point moves toward the leading edge and causes early trailing edge turbulent separation [13]. The extent to which roughness affects airfoil performance is dependent on the nature of the roughness, its size relative to the boundary layer thickness, the Re number and the airfoil type. Roughness destabilizes the laminar boundary layer and weakens the turbulent boundary layer in regard to adverse pressure gradients. The corresponding effects on airfoil lift and drag depend on the particular type of pressure distributions developed by the airfoil. The so-called laminar airfoils are particularly sensitive to roughness because the improved airfoil performance is obtained by tightly controlling the boundary layer behavior. Any deviations of the boundary layer from its intended behavior, such as that due to roughness, can result in significant deteriorations in performance.

To validate the aforementioned criterion, a 2D model was tested in a subsonic wind tunnel under steady state and plunging oscillatory motion.

.

II. EXPERIMENTAL APPARATUS

The experiments were conducted in the low speed wind tunnel in Iran. It is a closed circuit tunnel with rectangular test section of $80{\times}80{\times}200$ cm^3. The test section speed varies continuously from 0 to 100 m/sec.

Two models with 25 cm chord and 80 cm span were used. They are the critical section of a 660 kW offshore wind turbine blade. Both models are exactly identical and were constructed of fiberglass with a measured accuracy of ±0.1mm. One of the airfoil models is equipped with 64 pressure orifices on the upper and lower surfaces. The pressure ports are located along the chord at an angle of 20 degrees with respect to the model span to minimize disturbances from the upstream taps, Fig. 1. The unsteady aerodynamic loads were calculated from the surface pressure

F. Rasi Marzabadi, Aerospace Research Institute, Tehran, 14665-834 Iran (phone: +982188366030; fax: +982188362011; e-mail: rasi@ ari.ac.ir).

World Academy of Science, Engineering and Technology
International Journal of Aerospace and Mechanical Engineering
Vol:6, No:10, 2012

measurements along the chord. Another model is equipped with eight hot-film sensors. The hot-films are special version of the flush-mounting DANTEC probe, Glue-on type. The sensor is deposited on a KaptonTM foil with thickness of about 50μm which placed inside the fitted hole on the surface of the model in order to minimize the influence of probe thickness on transition. Its sensor is 0.9×0.1 mm and connected to a gold-plated lead area. The hot-films were located along the chord at an angle of 20 degrees with respect to the model span to minimize disturbances from the upstream one, Fig. 2. Hot-film data are obtained using constant temperature anemometer (CTA).

Data is transformed to the computer through a 64 simultaneous channel, 12-bit Analog-to-Digital (A/D) board capable of an acquisition rate of up to 1200 kHz.

To study the possible extent of performance loss due to the surface roughness, standard commercial grit (number 4 with thickness of 0.031mm) was used to simulate surface contamination. Surface roughness was applied at x/c=0.05 (near the leading edge of the airfoil) using a 12mm double stick tape along the airfoil span, Fig. 3.

The plunging oscillation system oscillates the model at various amplitudes with frequencies ranging from 1 to 4 Hz. It incorporates a crankshaft to convert the circular motion of the motor to the reciprocal motion, which is transferred to the model by means of rods, Fig. 4. The pitch rotation point is fixed at about the wing quarter chord which used only for setting the mean angle of attack of the airfoil in these tests. The plunging displacement was varied sinusoidally as $h = \bar{h}\sin(\omega t)$.

The plunging displacement was transformed into the equivalent angle of attack using transformation formula, $\alpha_{eq} = k\bar{h}\cos(2\pi ft) + \alpha_0$. Figure 5 shows an example of the variation of the equivalent angle of attack for one oscillation cycle with respect to its corresponding time history of the plunging motion. It can be seen that α_{eq} is a maximum or a minimum whenever $h=0$ during down-stroke or upstroke portions of the motion, respectively.

The experiments were conducted at Reynolds number of 0.42 million, and over a range of reduced frequencies from 0.03 to 0.11, at pre-stall, near-stall and post-stall regions. The data of aerodynamic loads were corrected for the solid tunnel sidewalls and the wake blockage effects using the method explained in Ref. 14.
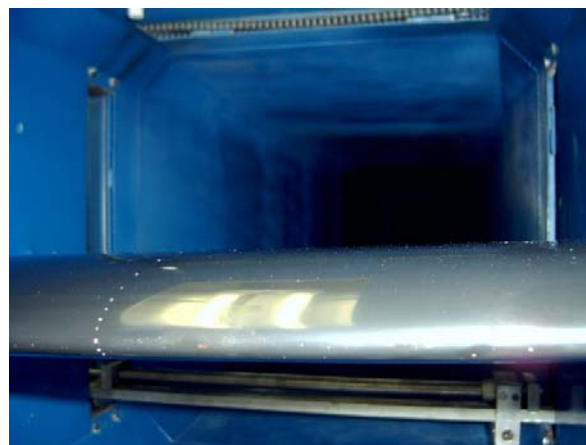

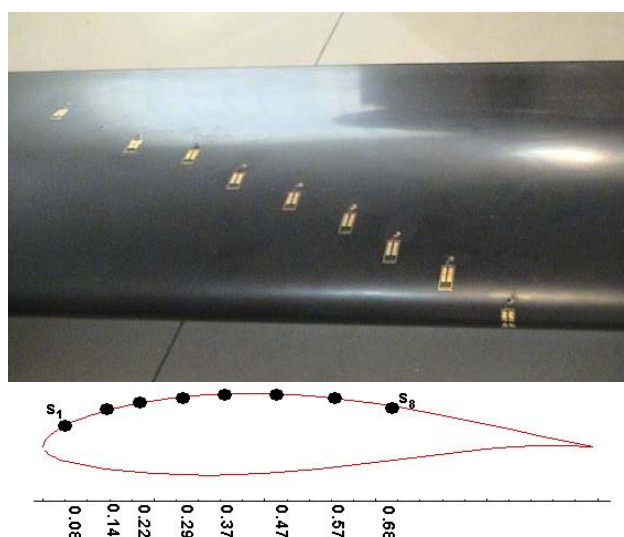Fig. 1 Airfoil model along with the location of the pressure ports

Fig. 2 Airfoil model along with the location of the hot-films

Fig. 3 Applied surface roughness

World Academy of Science, Engineering and Technology
International Journal of Aerospace and Mechanical Engineering
Vol:6, No:10, 2012

Fig. 4 Oscillation device

a) Plunging displacement

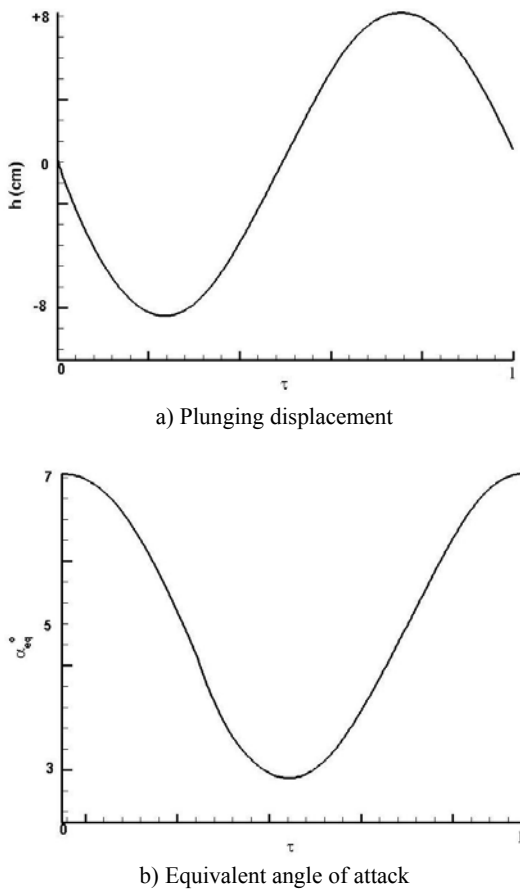

b) Equivalent angle of attack

Fig. 5 Time history of the plunging motion and its corresponding
equivalent angle of attack

III. RESULTS

Figure 6 depicts variations of the pressure coefficient with dimensionless time for nine upper surface pressure ports from the leading edge to the location of x/c=70%. The model is set to a mean angle of attack of 10 degrees and is oscillated at two different reduced frequencies of k=0.06 and 0.085. On the top of Fig. 6, the locations of the pressure holes and variation of the corresponding equivalent angles of attack with time are shown.

By inspecting Fig. 6a, it is seen that for pressure ports located at x/c<20%, the flow nearly follows the model motion and the resultant equivalent angle of attack and C_P data varies in a form of cosine type. The magnitude of C_P for all of the aforementioned ports decreases as τ increases reaching minimum value at $\tau\approx0.45$. However, the absolute values of C_P's are different at each port and decrease toward the trailing edge. However, for pressure ports located at x/c>20%, it is seen that the flow does not follow the model motion and $|C_P|$ remains almost constant during the entire cycle. It means that in this region of the airfoil surface, the pressure distribution does not change very much during the upstroke portion of the motion compared with those during the downstroke one. Note that the static stall angle of attack for this airfoil is 11 degrees [15] and for the present dynamic case α_0=10º and the model is oscillated around the static stall region.

For the higher reduced frequency case, k=0.085, Fig. 6b shows that for all pressure ports located at x/c>20%, the variations are similar to those of the lower reduced frequency one, however, $|C_P|$ for pressure ports located at x/c<20%, are slightly higher than those of Fig. 6a. By inspecting Fig. 6b, it is clearly seen that for the pressure port located at the leading edge, the magnitude of C_P does not decrease at τ=0, when the equivalent angle of attack starts to decrease. On the other hand, although the maximum equivalent angle of attack is at τ=0, but $|C_{Pmax}|$ does not occur at this time. For k=0.06, $|C_{Pmax}|$ occurs at $\tau\approx0.03$ while for k=0.085, this value occurs at $\tau\approx0.08$. This indicates that due to the oscillation frequency, the pressure distribution over the airfoil surface lags with respect to the change of the angle of attack. In fact, the ability of the flow to remember its past history is responsible for this phenomenon [8]. When the reduced frequency is increased, the model oscillates with higher frequency and so the lags between the equivalent angle of attack and the pressure distribution increases. This is called "pressure-gradient-lag effect" [16].
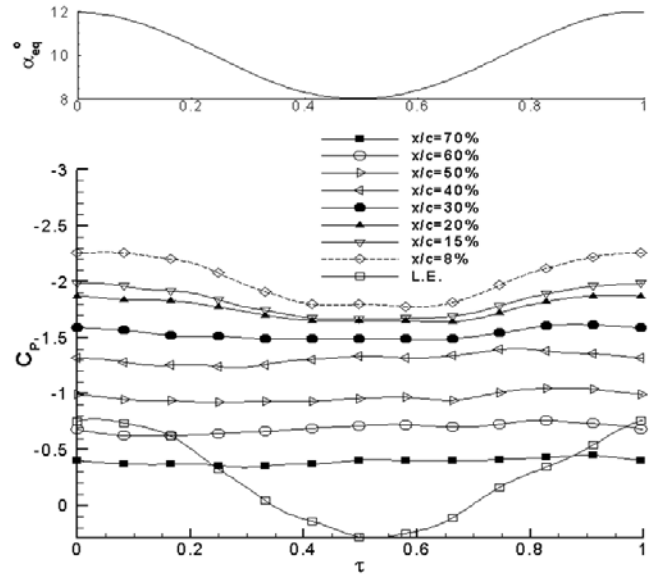
The effect of leading edge roughness on pressure distribution around the airfoil is presented in Fig. 7. The results are shown for three static angles of attack of 5, 10, and 18 degrees which are below, within and beyond the static stall angle of attack of the model, respectively. The transition location can almost be estimated from a sudden change in the slope of the pressure distribution which indicates the transition to turbulent through a separation bubble. The data clearly reveals that the flow transits as it passes over the roughness and becomes turbulent over the rest of the model. As indicated by arrows in Fig. 7a, at α=5°, the transition point moves from x/c≈0.55 to the roughness location at x/c=0.05, Fig. 7a. Note that the arrows are located at the beginning of the separation bubble, while in reality the flow becomes turbulent at a distance aft of the formation of the separation bubble. At higher angles of attack, it can be seen that the separated region over the model with roughness is more extensive than that of

World Academy of Science, Engineering and Technology
International Journal of Aerospace and Mechanical Engineering
Vol:6, No:10, 2012

the clean one, Fig's 7b and 7c. Furthermore, the absolute value of C_P on the upper surface for the model with roughness is less than that of the clean one in all angles of attack which results in a sharp reduction in the lift data.
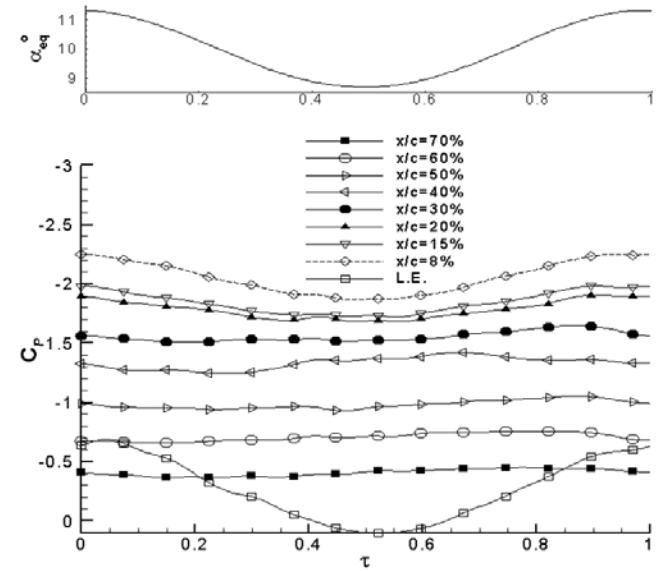
Figure 8 shows the composite dynamic plots of quasi-wall-shear stress, τ, calculated from un-calibrated hot-film signals in both clean and rough models. Variations of the equivalent angle of attack with time are shown on the top of the figures. The designated letters s1 through s8 shown on the right side of each trace are the hot-film responses in increasing order of chord wise positions, from about 8 to 68 percent of the chord. Based on the approach of Hodson [17] and Zhang [18], a quasi-wall-shear stress was defined as: $\tau = \left(\dfrac{E^2 - E_0^2}{E_0^2} \right)^3$.

Where E is the output voltage of the hot-film sensor and E_0 is the offset voltage, zero-flow voltage at the air temperature encountered during the test. In this figure the model is set to mean angle of attack of 10 degrees and oscillates with reduced frequency of 0.08 and plunging amplitude of ±8 cm. It is seen for the clean case that the signals of channels s1 to s4, have smooth response with time which represents the laminar flow up to about 30% of the chord during the entire oscillation cycles, Fig. 8a. Thickening of the boundary layer causes reduction of the shear stress toward the trailing edge. The near-zero values of channel s5 upholds the existence of laminar separation bubble at this location that causes transition of the boundary layer to occur further downstream toward the trailing edge. This is confirmed from the shear stress values of channel s6, which shows combinations of the laminar-turbulent flow. The values of shear stress vary from laminar to turbulent as the equivalent angle of attack increases during one oscillating cycle. As the equivalent angle of attack decreases, the flow again becomes laminar, Fig. 8a. The angles of attack in which the transition and relaminarization take place are not the same. The flow at the last two channels, s7 and s8, is turbulent since the magnitude of the shear stress is increased and further the fluctuation amplitudes are relatively high, too. For the rough model, Fig. 8b, it can be seen that there is no sign of laminar flow in any channels. Because the flow transits to turbulent as it passes through the roughness, even the signal of channel s1 show turbulent flow during entire one oscillating cycle. The quasi shear stress reduces toward the trailing edge due to thickening of the turbulent boundary layer. The outputs of channels after s6 toward the trailing edge show separated flow, Fig. 8b. Similar to the static result shown in Fig. 7, surface roughness causes early trailing edge turbulent separation in dynamic case.
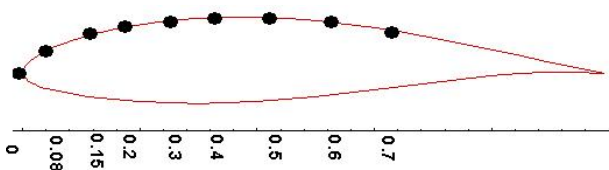

a) k=0.06

b) k=0.085

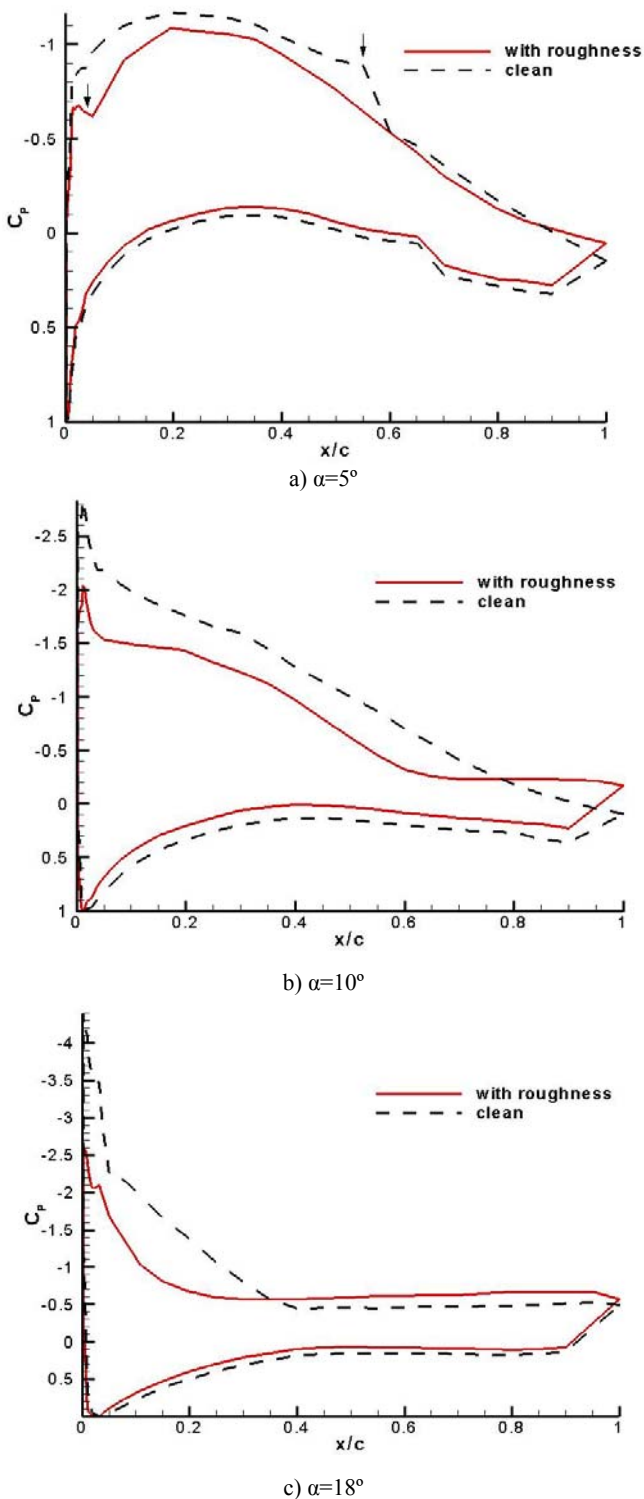Fig. 6 Variation of the upper surface pressure coefficient with non-dimentionalized time, $\alpha_0=10º$

World Academy of Science, Engineering and Technology
International Journal of Aerospace and Mechanical Engineering
Vol:6, No:10, 2012

a) α=5º

b) α=10º

c) α=18º

Fig. 7 The effect of leading edge roughness on the pressure distribution in static tests

a) Clean

b) With roughness

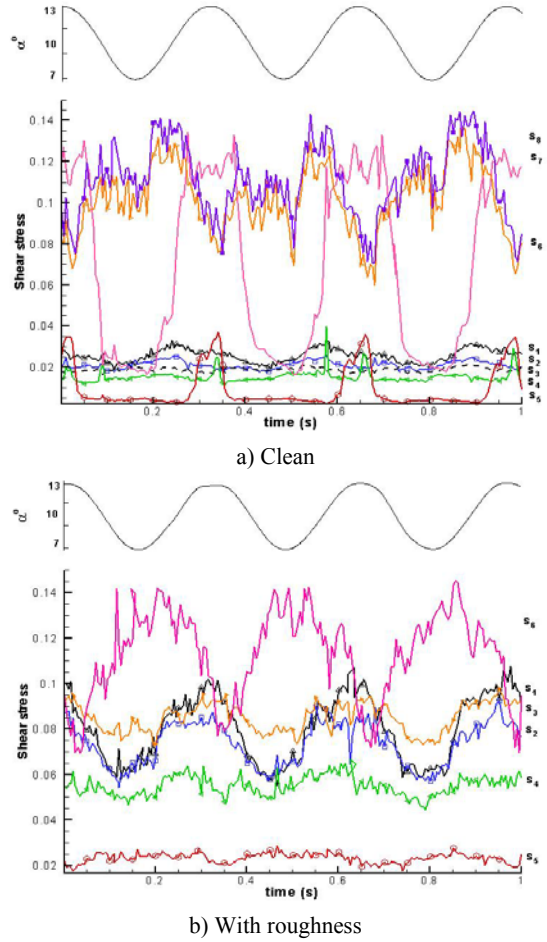Fig. 8 Time history of quasi-wall-shear stress, α_0=10º, k= 0.08

The unsteady aerodynamic loads were calculated from the surface pressure data, 64 ports, along the chord for both upper and lower surfaces of the model. The individual C_l, C_d and C_m hysteresis loops are shown in Fig. 9. The loads are shown for two different reduced frequencies of 0.06 and 0.085. An arrow gives the direction of each loop. The corresponding static values are also shown for comparison.

Figure 9a shows variations of C_l with the equivalent angle of attack. In the linear part of the static C_l values, the average slopes of the hysteresis loops tend to follow the steady data. The direction of the hysteresis loops is counterclockwise for both reduced frequencies. It means the lift in the upstroke motion lags its corresponding static value, while in the downstroke motion the reverse is true. As it is seen from Fig.9a, the effect of increasing the reduced frequency is to increase the induced angle of attack and widen the hystersis loops. Looking at Fig.9a, it is seen that oscillating the airfoil near its static stall region causes different trends in the dynamic lift coefficients. The hysteresis loops show a "figure eight" shape. This may indicate that there is an overshoot of the lift in the upstroke part of the curve at high equivalent angles of attack, while at low equivalent angle of attack, the reverse is true, undershoot. In fact the direction of the C_l hysteresis loops changes from lag to lead. The "cross-over"

World Academy of Science, Engineering and Technology
International Journal of Aerospace and Mechanical Engineering
Vol:6, No:10, 2012

point can be seen in this hysteresis loops. For k=0.06, it is around α=9.5°. But for k=0.085, it increases to an equivalent angle of attack of 11 degrees. Furthermore, increasing the reduced frequency induces higher maximum lift value and postpones the stall to higher equivalent angles of attack. Oscillating the airfoil with an incident angle of 18°, in the post stall region, causes the hysteresis loops of the C_l to become clockwise and wider. This is due to the influence of different time lags and vortex formations. As a fact, when oscillating the airfoil with lower mean angles, the direction of the hysteresis loops is strongly affected by the trailing edge wake and by the apparent mass effects. However, for the case when the model is oscillated with higher incidence, near static stall or beyond, there exists a wide separated flow region behind the airfoil and the dynamic stall vortex plays an important role in the trends of the hysteresis loops.

Figure 9b shows the C_d hysteresis loops. It must be noted that the drag coefficients here are only pressure drag of the airfoil which is calculated from the surface pressure data. The skin friction drag component was ignored in this figure; hence, the drag coefficient is underestimated. As the mean angle of attack increases, the average values of C_d increases too. The large-scale flow separation on the airfoil upper surface resulted in a very large circulation region in the wake of the airfoil. This will cause a significant aerodynamic drag force acting on the airfoil in the post stall region. The directions of the hysteresis loops are clockwise for all cases. It means that the dynamic pressure drag of the airfoil in the upstroke motion leads the downstroke one.

Figure 9c shows variations of the pitching moment coefficient calculated about $c/4$ of the airfoil with the equivalent angle of attack. The aerodynamic damping is computed from the area under the pitching moment hysteresis loop. The counterclockwise direction of C_m-α hysteresis loop indicates positive aerodynamic damping which results in stability during the plunging oscillation of the model [19]. In the pre-stall region, it is seen that there exists a few "figure eight" shapes in the hysteresis loops of the pitching moment curves, where one portion of the loop is traversed in a clockwise direction thus representing a negative damping contribution. However, the other portion has a counterclockwise direction, positive damping. When the mean angle of attack increases to α_0=10°, the Cm loops become counterclockwise that shows positive aerodynamic damping during the entire oscillation cycle. With further increase in the mean angle of attack, α_0=18°, where fully separated flow conditions exist, the loops change their direction to clockwise that results an instability during the oscillation.

Figure 10 shows a comparison between our test data and potential flow theory (Theodorsen's theory) [20] for the unstalled case. It is seen that at the same condition, there is qualitative agreement between the lift coefficient of the potential flow theory and our result. Note that Theodorsen's method is for a very thin airfoil while the present airfoil has a thickness ratio of about 16%.

The effect of roughness on unsteady lift coefficients is shown in Fig. 11. The hysteresis curves are for reduced frequencies of 0.044 and 0.07 for the clean and also rough cases. As it was mentioned on Fig. 7, using the roughness near the leading edge of the airfoil, results in reduction of the lift coefficients which reduces the effectiveness of the airfoil and also the rotor performance.
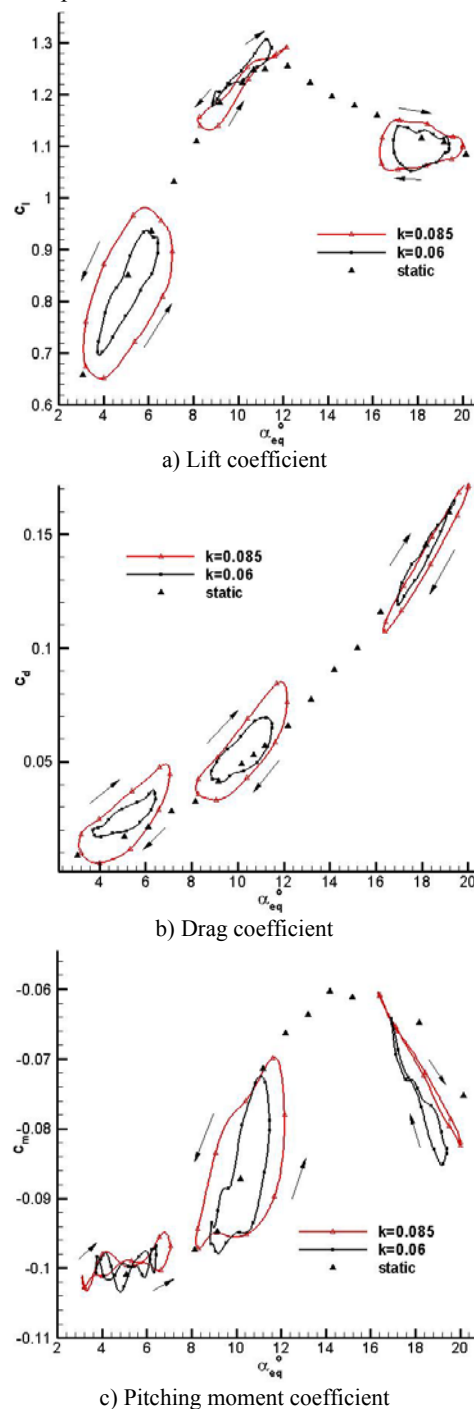

a) Lift coefficient

b) Drag coefficient

c) Pitching moment coefficient

Fig. 9 Variations of the aerodynamic coefficients with equivalent angle of attack

World Academy of Science, Engineering and Technology
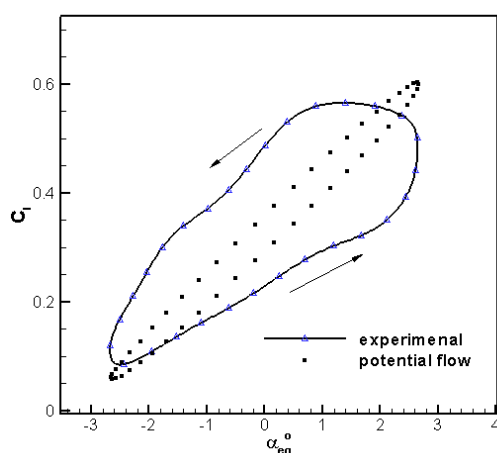International Journal of Aerospace and Mechanical Engineering
Vol:6, No:10, 2012

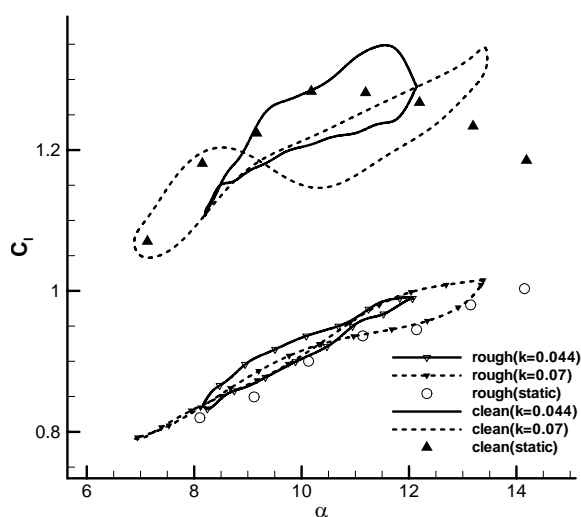Fig. 10 Comparison of the experimental data with the potential flow theory, k=0.058

Fig. 11 Effect of roughness on lift coefficient, $\alpha_0=10°$

IV. CONCLUSION

A set of experiments were conducted on an oscillating airfoil in the plunging motion. The experiments included measuring the surface pressure distribution and boundary layer state of the model for combinations of reduced frequencies and mean angles of attack. The unsteady aerodynamic loads were calculated using the surface pressure data. To simulate surface contamination on the wind turbine blade, the effect of leading-edge roughness on the state of the boundary layer and also aerodynamic coefficients was studied.

The measurements showed that increasing the angle of attack resulted in movement of the transition location toward the leading edge. Plunging the airfoil at higher mean angles of attack resulted in increasing the maximum suction over the airfoil and movement of its location toward the leading edge. There existed hysteresis between the transition location, which occurred by a laminar separation bubble, in the upstroke and in the down-stroke branches. Boundary layer transition occurred earlier for increasing rather than for decreasing the

effective angle of attack. Variations of the surface pressure coefficients and aerodynamic loads with the equivalent angle of attack showed strong sensitivity to reduced frequency and mean angles of attack due to the different influences of the pressure-gradient-lag and moving wall effects in addition to the vortex formations in the post stall regions.

Surface roughness moved the transition point toward the leading edge and caused early trailing edge turbulent separation which resulted in reducing the effectiveness of the airfoil.

REFERENCES

[1] Spera, D.A., "Wind Turbine Technology, Fundamental Concepts of Wind Turbine Engineering," *ASME Press, USA*, 1998, pp. 1-46.
[2] Bianchi, D.F., Battista, H.D., and Mantz, R.J., *Wind Turbine Control Systems*, Springer, Germany, 2007, pp. 8-30.
[3] Manwell, J.F., McGowan, J.G., and Rogers, A.L., *Wind Energy Explained Theory, Design and Application*, John Wiley and Sons Ltd, England, 2002, pp. 1-20.
[4] Tempel, V.D.J., "Design of Support Structures for offshore Wind Turbines," *PhD Thesis, Delft University of Technology, Netherland*, 2006, pp. 7-17.
[5] Jonkman, J.M. and Buhl, J., "Loads analysis of a floating offshore wind turbine using fully coupled simulation," *National Renewable Energy Laboratory, PhD Thesis, NREL*, USA, 2007, pp. 1-200.
[6] Leishman, J., "Challenges in modeling the unsteady aerodynamics of wind turbines," *AIAA 2002-0037, 21st ASME Wind Energy Symposium and 40th AIAA Aerospace Sciences Meeting, Reno, NV,* January 2002.
[7] Hansen, AC, Butterfield, CP, "Aerodynamics of Horizontal-Axis Wind Turbine," *Annual Review of Fluid Mechanics, Vol. 25,* 1993, pp.115-149.
[8] McAllister, K.W., Carr, L.W. and McCroskey, W.J. "Dynamic stall experiments on the NACA 0012 Aerofoil," *NASA TP-1100,* January 1978.
[9] Ericsson, L.E., and Reding, J.P., "Shock-induced dynamic stall," *Journal of Aircraft, Vol. 21,* May 1984, pp 316-321.
[10] Carr, L.W. "Progress in analysis and prediction of dynamic stall," *AIAA Journal, Vol. 25,* 1988, 1, pp. 6-17.
[11] Fukushima, T. and Dadone, L.U. "Comparison of dynamic stall phenomena for pitching and vertical translation motions," *NASA CR-2793,* July 1977.
[12] Rooij, RPJOM, Timmer, WA, "Roughness Sensitivity Considerations for Thick Rotor Blade Airfoils," *Journal of Solar Energy Engineering, Vol. 125,* 2003.
[13] Hu, Hui, Yang, Zifeng, and Igarashi, Hirofumi, "Aerodynamic Hysteresis of a Low-Reynolds-Number Airfoil," *Journal of Aircraft, Vol. 44, No. 6,* 2007, pp. 2083-2086.
[14] Barlow, J. B., Rae, W. H., and Pope, A., *Low-Speed Wind Tunnel Testing*, 3rd Edition, John Wiley & Sons, 1999.
[15] Soltani, MR and Rasi Marzabadi, F, "Effect of Plunging Amplitude on the Performance of a Wind Turbine Blade Section," *The Aeronautical Journal, Vol. 111, No. 1123,* 2007, pp. 571-587.
[16] Ericson, L.E., and Reding, J.P., "Unsteady Flow Concepts for Dynamic Stall Analysis," *AIAA Journal of Aircraft, Vol.21, No. 8,* Aug. 1984, pp. 601-606.
[17] Hodson, HP, and Howell, RJ, "Unsteady Flow: Its role in the Low Pressure Turbine," *9th International Symposium Unsteady Aerodynamics, Aeroacoustics and Aeroelasticity of Turbomachines*, Lyon, 2000.
[18] Zhang, XF, Mahallati, A, and Sjolander, SA, "Hot-Film Measurements of Boundary Layer Transition, Separation and Reattachment on a Low Reynolds Numbers," *AIAA 2002-3643, 38th AIAA/ASME/SAE/ASEE Joint Propulsion Conference & Exhibit*, 2002.
[19] Carta, F. A., "A Comparison of the Pitching and Plunging Response of an Oscillating Airfoil," *NASA CR-3172,* 1979.
[20] Theodoresen, T., "General Theory of Aerodynamic Instability and the Mechanism of Flutter," *NACA TR-496,* 1935.